Published in final edited form as:

Cell Rep. 2019 June 18; 27(12): 3447–3459.e3. doi:10.1016/j.celrep.2019.05.072.

Dynamic Modulation of Cortical Excitability during Visual Active Sensing

Annamaria Barczak[1,5,*], **Saskia Haegens**[1,2,3], **Deborah A. Ross**[1], **Tammy McGinnis**[1], **Peter Lakatos**[1,4], and **Charles E. Schroeder**[1,2,*]

[1]Translational Neuroscience Division, Center for Biomedical Imaging and Neuromodulation, Nathan Kline Institute for Psychiatric Research, Orangeburg, NY 10962, USA [2]Departments of Neurological Surgery and Psychiatry, Columbia University College of Physicians and Surgeons, New York, NY 10032, USA [3]Donders Institute for Brain, Cognition, and Behaviour, Radboud University, Nijmegen 6500HB, the Netherlands [4]Department of Psychiatry, New York University School of Medicine, New York, NY 10016, USA [5]Lead Contact

SUMMARY

Visual physiology is traditionally investigated by presenting stimuli with gaze held constant. However, during active viewing of a scene, information is actively acquired using systematic patterns of fixations and saccades. Prior studies suggest that during such active viewing, both nonretinal, saccade-related signals and “extra-classical” receptive field inputs modulate visual processing. This study used a set of active viewing tasks that allowed us to compare visual responses with and without direct foveal input, thus isolating the contextual eye movement-related influences. Studying nonhuman primates, we find strong contextual modulation in primary visual cortex (V1): excitability and response amplification immediately after fixation onset, transiting to suppression leading up to the next saccade. Time-frequency decomposition suggests that this amplification and suppression cycle stems from a phase reset of ongoing neuronal oscillatory activity. The impact of saccade-related contextual modulation on stimulus processing makes active visual sensing fundamentally different from the more passive processes investigated in traditional paradigms.

Graphical Abstract

*Correspondence: annamaria.barczak@nki.rfmh.org(A.B.), charles.schroeder@nki.rfmh.org(C.E.S.).

AUTHOR CONTRIBUTIONS

Conceptualization, C.E.S. and A.B.; Methodology, A.B., C.E.S., and P.L.; Data Collection, A.B., D.A.R., and T.M.; Analysis, A.B., S.H., and P.L.; Writing, A.B. and C.E.S.; Reviewing & Editing, A.B., S.H., P.L., and C.E.S.

SUPPLEMENTAL INFORMATION

Supplemental Information can be found online athttps://doi.org/10.1016/j.celrep.2019.05.072.

DECLARATION OF INTERESTS

The authors declare no competing interests.

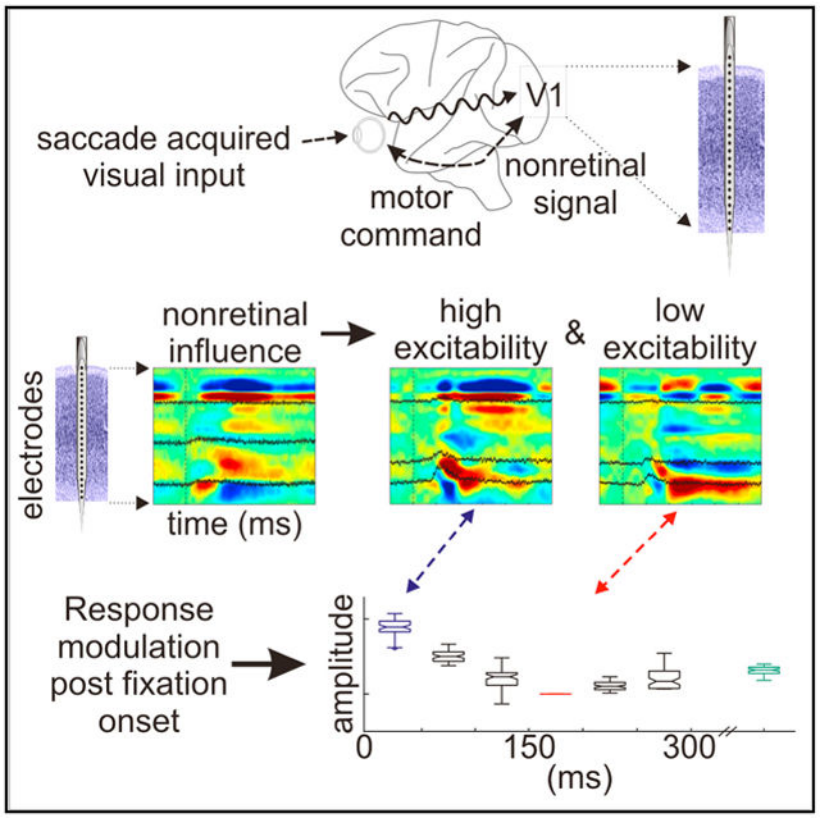

In Brief

By isolating contextual eye movement-related influences during active vision, Barczak et al. show that eye movements affect excitability in V1 such that responses are amplified immediately after fixation onset and suppressed as the next saccade approaches. This amplification and suppression cycle stems from a phase reset of ambient oscillatory activity in V1.

INTRODUCTION

“Active sensing” is a process in which sensory input that enters the brain is actively acquired by motor sampling (Kleinfeld et al., 2006; Schroeder et al., 2010; Hatsopoulos and Suminski, 2011) and is highly conserved across systems and species. Prime examples include whisking and sniffing in rodents (Deschênes et al., 2012), tactile and/or haptic exploration of objects (Hatsopoulos and Suminski, 2011), and saccadic sampling of visual scenes in primates (Yarbus, 1967; Maldonado et al., 2008). Common to all cases is that motor activity causes the stimulation of sensory receptors, which initiates the flow of information through the sensory pathways. This has several key implications. First, the information stream is shaped by the motor sampling pattern. Due to the saccadic sampling routine during visual exploration, the input stream is quantized into “volleys” of activity occurring rhythmically at 3–5 Hz (Rajkai et al., 2008; Melloni et al., 2009; Ito et al., 2011). This represents a chunking or parsing scheme that may be critical to sensory information processing but is largely unexplored. Second, it is believed that in parallel with each eye

movement, nonretinal signals are sent to cortical and subcortical visual areas to predictively prepare these areas for the impending sensory input volley. Whether this signal reflects a "corollary discharge" (Jeannerod et al., 1979; Wurtz and Sommer, 2004; Sommer and Wurtz, 2008), a top-down control signal related to temporal attention (Nobre et al., 2007; Schroeder and Lakatos, 2009; Morillon et al., 2014), or a combination of the two remains to be determined. Regardless, this nonretinal signal may transiently increase local neuronal excitability (Rajkai et al., 2008) and synchrony (Ito et al., 2011) at the onset of fixation just before the retinal input volley arrives in primary visual cortex (V1), potentially amplifying the subsequent V1 response. Third, during free viewing (FV) of complex scenes under photopic conditions, saccade-related stimulation of "extra-classical" receptive fields in the periphery may compound nonretinal modulation with a retinal component. Finally, there is indication that the mechanism underlying the eye movement-related fluctuation of neuronal excitability is a phase reset of ongoing oscillatory activity in both V1 (Rajkai et al., 2008) and higher-order area V4 (Zanos et al., 2015). This may be the most important effect of eye movement-related signals, as phase reset can promote the entrainment of neuronal dynamics to the saccade-fixation cycle that merges or embeds the content of each input volley into the context of ongoing activity in the visual system.

Due to technical difficulties inherent to studying visual processing while the eyes are moving, the classic approach to examining vision has been to analyze neuronal responses evoked by visual stimuli while gaze is held constant. Although the vast majority of basic vision research has been conducted this way, recent findings (Bremmer et al., 2009; Ibbotson and Krekelberg, 2011; Ito et al., 2011; Morris et al., 2012; Zanos et al., 2015,2016) indicate that it is possible to use active sensing tasks in which subjects explore visual scenes in more natural ways. One such study (McFarland et al., 2015) used a structured fixation-saccade task to minimize retinal input during the perisaccadic period and confirmed the basic temporal pattern of perisaccadic supression and enhancement of V1 firing observed previously with eye movements in the dark (Rajkai et al., 2008).

Building on this work, we devised a set of tasks that allowed us to first record neuronal responses to visual input during unconstrained FV and visual search and then effectively isolate the influences of contextual, eye movement-related signals in nonhuman primates. We analyzed laminar profiles of synaptic activity and concomitant neuronal firing (indexed by current source density [CSD] and multiunit activity [MUA], respectively) to document the temporal dynamics of the nonretinally mediated excitability fluctuation across the saccade-fixation cycle. Finally, we detailed the specific laminar frequency domain correlates of eye movement-related excitability modulation in V1. Our findings outline essential neurophysiological features of visual active sensing and point out a fundamental distinction between active vision and visual sensing in the absence of eye movements.

RESULTS

This study aimed to examine the potential effects that eye movement patterns have on visual processing while acquiring information as gaze shifts around a visual scene. Neuroelectric activity was recorded using 23-channel laminar electrode arrays. During each experiment, these arrays were acutely positioned to bracket the layers of V1 and sample field potentials

and concomitant MUA from all of the layers simultaneously. Penetrations were made in the foveal representation (0°–3° retinal eccentricity) of V1 in the lateral striate operculum.

As described in Method Details, two tasks were used to examine the influence of eye movements on retinal input processing. The first was a FV task in which images of naturalistic scenes were presented for 5 s, separated by 3-s periods of darkness. Figure 1A (top) shows an example image with a sample scan pattern overlaid. Figure 1B (top) shows the distribution of intersaccadic intervals (ISacI) during a single FV session. The total number of fixation-saccade pairs observed in this example was 839, with a median ISacI of 238 ms. The lack of task rules allowed each monkey to move its eyes at a naturally preferred rate. Across all of the FV experiments, the two subjects had median ISacI rates of 239 (SD: 10.5 ms) and 255 ms (SD: 35.8 ms). Although the naturally preferred eye movement rates were statistically different between monkeys across FV experiments (two-sample t test, $p < 0.001$), the observed median eye movement frequencies were 4.2 and 3.9 Hz, respectively, which were both within the delta frequency band and within the range of previously reported eye movement rates (Rajkai et al., 2008; Melloni et al., 2009; Ito et al., 2011).

Ideally, to isolate nonretinal components, activity related to eye movements made in complete darkness would be examined. However, in this condition, eye movement rates radically decreased (Figure 1B, center) and ISacI variability increased. To circumvent this drastic decrease in engagement with the environment, we used a “gray screen search” (GSS) task that allowed us to study the effects of saccades in the absence of direct foveal stimulation while maintaining an active behavioral state and a high rate of saccades. During GSS, eye movements occurred on a screen with a uniform blank gray background. While this largely eliminated eye movement-related fluctuations of foveal visual input, it does leave open the possibility of peripheral, extra-classical receptive field stimulation. In a representative GSS session (Figure 1B, bottom), median ISacI was 328 ms (SD: 133.5 ms). Across GSS experiments, eye movement dynamics were consistent between monkeys (two-sample t test, NS; not significant). Median ISacI for each monkey was 333 (SD: 12.3 ms) and 339 ms (SD: 19.0 ms), which corresponded to eye movement rates of 3.0 Hz, which is within the delta range.

Both the FV and the GSS tasks elicited robust eye movement patterns, although there was a difference in ISacI between the tasks. Eye movements during the GSS task were slower (median ISacI: 335 ± 14.0 ms) than those during FV (median ISacI: 241 ±23.7ms; two-sample t test, $p < 0.001$). While statistically different, in both cases the eye movements occurred within the delta range (3.0 and 4.2 Hz) and were therefore still comparable. We could directly analyze the dynamics of eye movement-related signals while the gaze moved across visually rich images (during FV) and in the absence of eye movement-related changes of foveal visual input (during GSS).

Temporal Dynamics of Eye Movement-Related Laminar Activation Patterns

Given that viewing behavior and gaze direction were unconstrained, we analyzed only activity related to a subset of eye movements. After approximating the receptive fields of the neuronal population at the recording sites (see Method Details and Figure 2), only trials with eye movements that began and ended within this central portion of the screen (Figure 1A,

yellow box) were analyzed. With this selection criterion, we examined fixation- and saccade-related profiles for eye movements with receptive fields within the visual field confines of the monitor and avoided contamination of these profiles with foveal visual responses to the edges of the computer monitor.

We captured eye movement dynamics by analyzing neuronal activity with respect to two prominent events: fixation and saccade onset. Averaged CSD and MUA laminar profiles, time locked to each event, outline robust fixation-related (Figure 3, top) and saccade-related (Figure 3, bottom) modulation of transmembrane current flow and neuronal firing in local neurons. Since information about anatomical connections can be used to infer how information is transferred between areas (Felleman and Van Essen, 1991), these laminar CSD profiles, which reflect net transmembrane current flow across layers, can be examined in conjunction with eye movement-related MUA to determine whether the eye movement-related activity we observed had driving (action potential generating) or modulatory (subthreshold) effects. Profiles from driving inputs typically show an earlier CSD and MUA activation in the granular layers (layer 4) followed by activation in supragranular and infragranular layers. Profiles from modulatory inputs tend to show an earlier CSD response in the extragranular layers (supra- and infragranular) and do not necessarily lead to increases in MUA (Givre et al., 1994; Schroeder et al., 1998).

The FV example (Figure 3, left) shows a strong modulation of excitability tied to both eye movement events. This was not surprising given that strong retinal input occurred at each fixation, which drove feedforward activation (early current sink and MUA increase in granular layer 4, which spreads to the extragranular layers). In comparison, the saccade-triggered profile shows earlier activation in the extragranular layers. Similarly robust profiles of fixation- and saccade-related activity were observed during the GSS condition (Figure 3, right), when there was no change in the “preferred” retinal input related to either eye movement onset. In this GSS condition, however, both fixation- and saccade-related CSD activity profiles show non-feedforward patterns, which have an initial synaptic activation beginning outside of granular layer 4.

Quantification of laminar onset latency patterns (Figure S1) revealed systematic differences between fixation- and saccade-locked profiles and between FV and GSS profiles. All of the comparisons in this section were statistically evaluated using the Kruskal-Wallis test with a multiple comparison analysis (Tukey’s test). As previously mentioned, during FV, the fixation-locked profile had a characteristic “feedforward” pattern with significant delays between the initial activation of granular layer 4 and the later activation of the supragranular and infragranular layers. There was no difference in the latencies between supragranular and infragranular layers. In the same condition, the saccade-locked profile was distinctly different from a feedforward pattern. At saccade onset, the activation of granular layer 4 was significantly later than that in the extragranular layers, and there was, again, no difference between onsets in the supragranular and infragranular layers. In contrast to the FV task, during the GSS, there was only one pair of layers that showed an onset latency difference for fixation-locked data and there were no systematic CSD onset latency differences between any of the layers for saccade-locked data.

To quantify eye movement-related modulation of local neuronal excitability via CSD amplitude, we calculated a depth of modulation value (the difference between baseline amplitude and peak CSD values) for each layer and condition and compiled these values across experiments (Figure S1B). During FV, the depth of modulation in the supragranular and infragranular layers was significantly greater than that in the granular layer for fixation- and saccade-related activity. There was no difference in the modulation of amplitude between supragranular and infragranular layers fo fixation- or saccade-related activity. During GSS, there were fixation- and saccade-related differences between several layer combinations (fixation: supra versus gran and gran versus infra; saccade: supra versus gran, supra versus infra, and gran versus infra).

Considering the strong retinal input during FV, we expected that the amplitude modulation observed would be greater than that during the GSS. For both saccade- and fixation-related profiles, the depth of modulation within the granular and infragranular layers was significantly greater in the FV condition than in the GSS condition (all two-sample t tests, $p < 0.001$). However, the supragranular depth of modulation values did not statistically differ between tasks.

To summarize, fixation-locked activity during FV produced the only activation profile that had a typical feedforward, driving input pattern. This was likely due to the volley of strong driving input coming into the visual system through the retina at each fixation. The remaining three profiles (saccade locked during FV, as well as both fixation and saccade locked in the GSS condition) had non-feedforward characteristics consistent with their being initiated by modulatory inputs rather than driving inputs.

Transient Excitability Modulation of Visual Neurons

To sample excitability at different time points during the saccade-fixation cycle, we analyzed only the Gabor-evoked responses that occurred while monkeys fixated within the previously determined portion of the screen during GSS. Stimulus-evoked responses were grouped based on the time difference between fixation and flash onset (Figure 4B). If eye movements cyclically influence visual processing, then examination of stimulus-evoked responses just after fixation (group 1 [grp1]) and roughly halfway through a fixation-saccade cycle (grp4) should show the largest qualitative and quantitative differences. Stimulus-evoked CSD response profiles for grp1 and grp4 (Figure 4C) show that the current source and sink configurations in the supragranular layers differed between these groups. Responses in grp1 have a source-over-sink configuration that is typical for feedforward activation of the supragranular laminae (Schroeder et al., 1991, 1998), while grp4 responses have a more rapidly alternating and atypical sink-over-source pattern. CSD and MUA amplitudes were also reduced throughout the layers in grp4 relative to grp1 (Figures 4C-4E). Example laminar MUA averages (Figure 4D) show that the response amplitude between 40 and 90 ms post-flash was the greatest when the flash occurred closest to fixation onset. The response amplitudes of grp4, which includes responses to flashes that occurred about halfway through one eye movement cycle, was smaller even when compared to grpAll.

To further detail the cyclical nature of these eye movement-related effects (Figure 4E), across all of the experiments, we statistically examined the effect of time between stimulus

and fixation onsets by comparing stimulus-related MUA across all of the response groups and for all flashes regardless of timing (grpAll). Since the timing of the visual stimulus is random with respect to fixation onset, the grpAll condition cancels out saccade-related modulation and provides an approximation to the condition in which stimuli are presented during held fixation. Comparisons showed that response amplitude was largest in the groups closest to fixation onset. Using Kruskal-Wallis tests and multiple comparison analyses, each individual group was compared to one another (results in Figure 4 legend). Amplitudes in grp1 were significantly larger than those in grp3, grp4, grp5, and grp6 across all of the layers. For the first four groups, as the time between the stimulus and fixation onsets increased, the evoked response decreased. Stimulus-related response amplitudes began to increase again 200–300 ms post-fixation onset (grp5 and grp6).

While the cyclical shape of the overall excitability modulation was visually evident across experiments (Figure 4E), it is also important to note that across all layers, responses to flashes that occurred closest to fixation onset were also statistically greater than the average response to all Gabor flashes (supra: grp1 versus grpAll $p < 0.01$, gran: grp1 versus grpAll $p < 0.001$, and infra: grp1 versus grpAll $p < 0.01$). These comparisons highlight the important effect that eye movement timing has on stimulus processing, which results in stimuli occurring closest to fixation onset having the largest normalized MUA response.

Eye Movement-Related Modulation of Ongoing Activity

Results presented thus far show that contextual modulation leads to an increase in excitability and a response amplitude enhancement across the layers of V1 for ~100 ms after fixation onset, which highlights the relevance of events that occur during the natural saccadic sampling of a visual scene. Given the cyclic nature of the post-fixation excitability modulation, we next examined oscillatory dynamics to investigate the underlying mechanism of this contextual eye movement-related excitability modulation.

We computed the eye movement-related power spectra and intertrial coherence (ITC) during the FV task and aligned the data to either fixation onset (Figures 5A and 5B) or saccade onset (Figures 5D and 5E). Power and ITC fluctuations (pre- versus post-eye movement) were statistically compared within delta (1.0–3.8 Hz), theta (4.1–7.5 Hz), and alpha (9.3–13.0 Hz) frequency bands (Figures 5C and 5F). While viewing natural images, there is a volley of visual input that courses into the system from the retina during each fixation. Such volleys elicit stimulus-evoked responses across visually relevant cortical areas. As expected with typical stimulus-evoked responses, we observed broadband power and ITC fluctuations across frequencies <70 Hz and across layers. Despite these large broadband power fluctuations, there was no statistically significant eye movement-related difference in power within any frequency band or across any layer. However, we did find a significant eye movement-related difference in phase concentration. Significant increases in theta and alpha ITC were observed across all layers, whether data were aligned to fixation or saccade onsets (Wilcoxon rank-sum tests with Bonferroni correction, $p < 0.05$).

Peak frequencies within these broadband activity changes showed several interesting dynamics. The most obvious is the highly variable peaks of power in the delta band (~2.4 Hz) that were confined to the supragranular layers and did not have a significant ITC

correlate. Theta phase concentration was more heavily weighted in the granular and infragranular layers, and the peak theta frequency was consistent between all of the layers for fixation-related activity (all layers: 5.1 Hz) and the lower layers for saccade-related activity (gran: 4.8 Hz, infra: 5.1 Hz). This theta frequency is slightly higher than the corresponding rate of eye movements (4.2 and 3.9 Hz for monkeys 1 and 2, respectively). Although alpha activity was present across all of the layers, the peak alpha frequency in the compiled ITC (Figures 5B and 5E, right column) decreased between supragranular and infragranular layers for fixation-aligned (11.0–9.3 Hz) and saccade-aligned activity (13.0–10.4 Hz).

Spectral peaks were temporally shifted between fixation- and saccade-locked conditions. To quantify this shift, we calculated the timing of the alpha amplitude peak for both sets of eye movement-related data within the 0- to 200-ms period post-eye movement onset. The median timing of the alpha amplitude peak in the fixation-related activity occurred 35, 35, and 30 ms earlier than the peak in the saccade-related activity in the supragranular, granular, and infragranular layers, respectively. These differences were statistically significant (Wilcoxon rank-sum test with Bonferroni correction, all $p < 0.001$). Significant ITC peak differences (20, 20, and 15 ms, respectively) also occurred between eye movement type in the supragranular ($p < 0.05$), granular ($p < 0.001$), and infragranular ($p < 0.001$) layers.

To evaluate the spectral impact of isolated contextual inputs, we conducted the same single-trial wavelet analysis on the eye movement-related activity during the GSS task when the monkey was moving its eyes over a uniform, blank gray screen. The absence of a direct visual input in this case was particularly obvious in the power spectra of the granular layer (Figures 6A and 6D). In contrast to the spectral profile of the granular layer during FV (Figures 5A and 5D), there was little sign of a broadband power fluctuation. Even in the absence of a direct evoked response, however, there were still power fluctuations in the supragranular and infragranular layers in frequencies below the low gamma range. The delta, theta, and alpha peaks that were noted during FV persist in the absence of a strong visual input. When compiled across experiments, these power dynamics were most strongly evident in the supragranular layer, with peaks in the delta range. The persistent wide range of delta power peaks likely indicates that supragranular neuronal activity is dominated by ongoing oscillations, while the strongest visual input-related responses occur in the granular and infragranular layers. Clear power peaks were less evident in the granular and infragranular layers, regardless of the eye movement event to which the data were aligned.

For eye movements made during the GSS task, ITC spectra (Figures 6B and 6E) revealed narrower bands of phase concentration compared to those made during FV. The alpha peaks previously seen in the FV data across layers were no longer clearly defined in the granular and infragranular layers. Despite less clear peaks across the experiments, when aligning the data to either fixation or saccade onset, there was a statistically significant eye movement-related increase in phase concentration in the theta range within granular and infragranular layers (Wilcoxon rank-sum tests with Bonferroni correction, $p < 0.01$). Significant alpha ITC was seen in the extragranular layers ($p < 0.05$). Saccade-aligned activity showed significant phase concentration within both theta and alpha ranges across all of the layers ($p < 0.05$) while lacking corresponding increases in theta or alpha power.

The median eye-movement rates for the two monkeys during this task were both ~3.0 Hz. Across experiments, the peak ITC within the delta frequencies was observed in the fixation-related grouped data at 3.6, 3.6, and 3.3 Hz and in the saccade-related data at 3.1, 3.6, and 3.3 Hz from supragranular to infragranular layers.

As previously discussed, when monkeys were placed in complete darkness, their eye movement patterns changed dramatically—fewer overall eye movements and increased ISacI. However, since there was less variability between saccade durations across conditions, to verify that the observed effects were evident while the monkey was in complete darkness, we analyzed the activity associated with a subset of saccades made in the dark. Examination of the power distribution for these selected saccades (Figure 7A) shows that although there is a broad increase in power across frequencies, the distribution is different from that observed with an evoked response (Figure 5A). Compiled data collapsed across experiments show that there is, again, a great variation in power within the delta band. This broad power variation is observed at 2.3 Hz, which is slower than the overall rate of eye movements observed in either the FV or the visual search conditions and is in line with the changes in eye movement dynamics previously described. In the dark, peak delta ITC frequencies are 4.1, 2.6, and 3.1 Hz across supragranular, granular, and infragranular layers, respectively (Figure 5B), and peak alpha ITC can also be observed in the supragranular and infragranular layers (peak: 13.0 Hz). When examining phase concentration before and after saccade onset (Figure 7C), there is a significant increase in theta ITC across all layers and an increase in alpha ITC in the supragranular layer alone ($p < 0.01$).

DISCUSSION

The results of this study highlight the dynamic nature of natural active vision and the effects of cyclically occurring eye movements on ambient neuronal dynamics and excitability in V1. We find that, first, the activation of visual cortex by input acquired during “active” FV produces a feedforward activation profile that resembles the profile driven by stimuli that are presented to the system in a traditional “passive” paradigm during sustained visual fixation (Schroeder et al., 1991; Maunsell and Gibson, 1992; Mehta et al., 2000a, 2000b). However, systematic comparisons of laminar response profiles at time points after fixation (Figures 4 and S1) suggest that the two methods whereby visual input is acquired—passive versus active—may differ fundamentally. This point is amplified by the recent finding that during visual fixation, sensory gain modulation due to sustained spatial attention to peripheral locations is tightly coupled to microsaccades toward the attended location (Lowet et al., 2018). Second, we were able to isolate and define the physiological impact of the eye movement-related contextual signal during the performance of a visual search task. The contextual signal was tied to a significant modulation of excitability that cycled from enhancement immediately after fixation onset to suppression in the period preceding the next saccade. Third, we showed that eye movements can reset the phase of ongoing neuronal oscillations, resulting in their entrainment, which can lead to the predictive modulation of excitability and enhancement of stimulus processing (Lakatos et al., 2008, 2013). These findings combine with earlier reports (Lowet et al., 2018; Zanos et al., 2015, 2016; Bosman et al., 2009) to suggest that the complete understanding of visual processing in primates requires that active eye movement dynamics be considered.

Contrasting Dynamics of Active Sensing and Passive Vision

Responses to stimuli presented just after fixation (grp1) and responses to all stimuli presented during fixations (grpAll) provide a reasonable approximation of the differences between natural active vision and vision as it is typically studied, with stimuli presented to subjects that are required to maintain gaze fixation. As depicted in Figure 4, neuronal firing patterns (indexed by MUA amplitude over time and across all layers) differ quantitatively between grp1 and grpAll. In this regard, natural active vision appears fundamentally different from the visual process that we typically study when presenting stimuli passively to an observer during sustained fixation.

Our analysis highlights a suppressive state whereby the response to visual stimuli presented ~150–200 ms post-fixation (grp4) is significantly smaller than when stimuli are presented immediately after fixation onset. The supragranular layers of the grp1 and grp4 CSD profiles are qualitatively different: the major source ad sink configurations at the time of the visual input arrival are opposite in sign. Example profiles (Figure 4C) show a source-over-sink pattern just before 0 ms in the grp1 colormap and an opposite pattern for grp4, indicating that net excitability in the local neuronal ensemble is trending in opposite directions between these two groups. In addition, the time course and frequency of the supragranular source-sink alternation differs between active and suppressive states. These temporal variations suggest that there is a difference in the membrane conductance and that different time constants are engaged (Vijayan and Kopell, 2012; Carracedo et al., 2013; Lee et al., 2013).

Laminar Profile and Origin of Contextual Influences

The most prominent increases in power and phase concentration related to fixations and saccades in the absence of eye movement-related fluctuation of foveal visual input (in the GSS condition) were observed in the extragranular layers (Figure 6). The strong weighting of the contextual modulation toward the extragranular layers indicates that this signal does not originate in the main relay neuron populations (lateral geniculate nucleus [LGN], the P and M cells) and does not feed forward into V1. Since the main relay neuron (parvo- and magnocellular) inputs target mainly layer 4c of V1 (Felleman and Van Essen, 1991), this extragranular targeted pattern of activity likely originates elsewhere. Given the laminar pattern of the saccadic modulation and the fact that it clearly entails a change in the net excitability of the V1 neuron population, it appears that this signal reflects modulatory input from another source that could include either a higher-order cortical area (i.e., a top-down effect) or a subcortical source outside of the main geniculostriate relay systems. Likely subcortical origins include the pulvinar complex, whose modulatory components project to extragranular cortical layers (Sherman and Guillery, 2002) and the “matrix” (koniocellular) thalamic pathways that project mainly to the most superficial layers of V1 (Casagrande, 1994; Jones, 2001). In the case of the latter target, it would reconcile our findings with a previous study (McFarland et al., 2015) that suggested that nonretinal modulation effects are fed forward from LGN to V1.

Linkage of Modulatory Effects to Eye Movement Components

It has been suggested that saccadic modulation effects are more closely tied to saccade onset than to fixation onset (Lee and Malpeli, 1998; Maldonado et al., 2008; Ito et al., 2011). Our

findings support this view in several ways. First, when strong foveal visual stimulation was present (during FV), the trial-averaged laminar CSD profile time locked to fixation onset is best described as feedforward, which means that initial activation is located in the major thalamo-recipient layers of V1 (4C) and are followed by activity in the extragranular layers. The laminar CSD and MUA profiles time locked to saccade onset clearly contrast with this description since the initial activity occurs in extragranular sites. Second, in the GSS condition, which was designed to isolate contextual eye movement-related effects, phase concentration estimates showed higher ITC values and more distinct spectral distributions for saccade-aligned than for fixation-aligned activity (compare Figures 6B and 6E). Saccade-aligned ITC patterns revealed phase concentration in distinct portions of the theta and alpha bands within the supragranular and infragranular layers, but ITC peaks were generally less clear for fixation-aligned activity. If the modulatory signal is linked to saccade onset, then the robust fixation-related laminar activation profile observed could be due to the rather stereotypic (35–50 ms) duration of saccades.

Functional Significance of Modulatory Signals

Eye movements shift gaze and sample information from different parts of the visual environment (Yarbus, 1967). Spatial selective attention can also be used to sample the visual world by covertly shifting attention while the gaze is held constant. However, most of the time, the orientation of visual attention is yoked to the direction of the gaze (Sheliga et al., 1994; Hoffman and Subramaniam, 1995; Deubel et al., 1996). The short latency modulatory signal that we have studied here could reflect either a corollary discharge sent by the motor system to prepare visual areas for the impending visual input (Sommer and Wurtz, 2008), a top-down control signal related to spatial attention (Noudoost et al., 2010), or a mixture of the two. Functional MRI data collected while humans performed tasks requiring covert and overt attentional shifts have shown that there is overlap between oculomotor and attention processes (Sheliga et al., 1994; Corbetta et al., 1998). Lowet et al. (2018) further emphasized the tight link between attention and eye movements, showing that covert attention-related modulation in macaque V4 and inferior temporal (IT) cortex is coupled to the onset of the microsaccades that occurred during sustained fixation. The present study does not distinguish between attentional and corollary discharge classes of effects. While it is possible to design tasks that can forge this distinction, this will require additional experimentation. In the present case, given that the monkeys were engaging in voluntary behavior and that attention can shift at about the same rate as the eye movements we observed (Landau and Fries, 2012; Fiebelkorn et al., 2013), it is likely that dynamic shifting of spatial attention is yoked to macrosaccades, as it is to microsaccades (Lowet et al., 2018). Nonetheless, it is important to keep in mind that whether the contextual signal is considered to be attention or corollary discharge related in nature, it likely plays a key role in natural visual processing.

As reported previously (Bosman et al., 2009), small correctional eye movements during sustained fixation (microsaccades) (1) occur at rates like those reported here, (2) are similarly rhythmic, and (3) produce a local phase reset. Thus, it is likely that the effects of saccades are generally similar, irrespective of their magnitude. However, this question remains of interest, as does the question of the directionality of any eye movement relative to

peripheral receptive fields (Zanos et al., 2015) and attended targets (Lowet et al., 2018). We also need to understand the extent to which the effects of nonretinal cues associated with smooth pursuit eye movements differ from those of saccades. Although beyond the scope of the present study, this larger set of questions is central to our continuing studies.

Shaping Ongoing Activity to Optimize Input Processing—The most obvious effect of saccade-related modulation in V1 is the amplified neural representation of visual stimuli that appear in the center of the gaze at fixation onset. From a system-design perspective, this enhancement effect makes sense because objects targeted by saccades are by definition task relevant and merit priority in visual processing. The cyclical excitability fluctuation in V1 is consistent with this functionality because the high excitability state occurs shortly after fixation onset and cycles down to a low excitability state just before initiation of the next saccade (Figure 4). As suggested by Lowet et al. (2017), we predict that there would be a facilitation of information transmission between cortical areas also linked to the saccade-fixation cycle. There is prior evidence that eye movement-related excitability modulation occurs in the higher-order visual cortex (Purpura et al., 2003; Zanos et al., 2015, 2016), as well as in LGN (Reppas et al., 2002; McFarland et al., 2015). If the pattern of excitability increasing just after fixation and decreasing just before the next saccade is common to many or all visual areas, then there would be increased coherence between visual areas at a frequency corresponding to the rate of eye movements (3–4 Hz).

Enhancement of Information Encoding—Another possible effect concerns the spike-phase coding of information, like that described for auditory cortical processing (Kayser et al., 2009). While our study was not designed to investigate this issue, it is worth considering how spike-phase coding may operate in visual processing. First, the elements that make up a complex visual scene include both high- and low-contrast edges, as well as a range of object colors that differentially activate the major afferent (P, M, and K) streams in the geniculostriate pathway. Second, these parallel afferent channels convey retinal input into V1 at different speeds, with M afferents generally conducting faster than P afferents (Morrocco and McKlurkin, 1982; Schiller and Colby, 1983; Schroeder et al., 1989, 1998). K neurons are generally regarded as being slowly conducting (Fries, 1981; Yukie and Iwai, 1981; Hendry and Yoshioka, 1994), despite cell body size and axon caliber data (Hendry and Reid, 2000), which suggests that K populations may also include rapidly conducting neurons. Third, across afferent streams, response latency is systematically related to stimulus contrast. Putting these facts together with the readily apparent pattern of sustained multiunit firing over the initial half (~100 ms) of the fixation-saccade cycle (Figure 4), it is reasonable to presume that different types of information encoded by each stream would trigger V1 neuron firing at characteristically different phases of the ongoing 3–4 Hz oscillation caused by the eye movement-related rhythmic pattern of nonretinal input. While the proposed latency grouping of different types of information and the presence of a clear reference rhythm do not guarantee that spike-phase coding will occur in V1, or that there will be areas downstream of V1 that have access to the reference rhythm and can thus “read” the code, it is evident that conditions supportive of spike-phase coding exist in V1.

Perceptual Enhancement of Visual Inputs—Psychophysical studies have shown not only that perceptual sensitivity increases at fixation (Burr et al., 1994) but also that perceptual onset time, the perception of a new stimulus pattern, begins at the end of a saccade (McConkie and Loschky, 2002).

Implications Regarding the Functional Significance of the Alpha Rhythm

A striking feature of the neuronal dynamics associated with eye movements that occur in lieu of related retinal input changes (Figure 6) is the prominence of alpha band effects despite the modulated alpha frequencies not being directly or harmonically tied to the eye movement rate. Regarding laminar distribution, saccade-related alpha activity is strongest in the supragranular layers, just like spontaneous alpha oscillations (Haegens et al., 2015). The pattern of phase concentration effects apparent in the ITC plots, particularly in the supragranular layers, suggests that alpha-range activity is reset by the nonretinal signals of each saccade and thus aligns the alpha phase to these events. Considering the proposition that alpha reflects “pulsed inhibition” (Jensen and Mazaheri, 2010; Mathewson et al., 2011), the pattern of alpha-power modulation is paradoxical; the model suggests that an alpha-power increase is associated with a decrease in neuronal firing (i.e., an excitability decrease; Haegens et al., 2011). However, we do not detect a significant modulation of alpha power along the lines predicted by the pulsed inhibition model. If anything, the visible trend appears to be in the opposite direction–increase in alpha power associated with increase in multiunit activity.

Related to this issue, an earlier paper by Zanos et al. (2016) reported that alpha-power increases in V4 were potentially related to saccadic suppression, but were specific to electrodes recording from peripheral retinal representations. This effect may also occur in V1, but it would have been missed in our study as we only recorded from sites representing the fovea. Also potentially related to a suppressive role for alpha, a recent paper by Bastos et al. (2018) concluded that in prefrontal areas, lower-frequency (4–22 Hz) activity in the lower cortical layers had a broad suppressive influence on higher-frequency activity in superficial cortical layers. While the 4- to 22-Hz range includes the alpha as well as the surrounding theta and beta bands, this type of effect does not appear to be mirrored in our sample of V1 activity. Rather, across all layers, saccade-related amplitude and phase modulations throughout the 4- to 22-Hz range appear to be associated with a general increase in the amplitude of higher-frequency activity up to the range of neuronal firing (MUA). Further study will be required to sort out several potential explanations for the divergence between our results and those of earlier studies concerning alpha-range effects.

One explanation that may reconcile these observed differences is based on the proposition that a single cycle of alpha reflects a cortical ensemble “duty cycle” (Gips et al., 2016). When a cortical ensemble (column or group of columns) is activated, a large fraction of the neurons responds in a coherent fashion, and it takes ~100 ms for the ensemble activation to run its course and return to a baseline excitability state. The widely observed coupling of neuronal firing to alpha phase (Haegens et al., 2011, 2015; Saalmann et al., 2012) also fits with this idea. We speculate that, as in the present case, when yoked to sensory processing by phase reset and entrainment, alpha band dynamics become part of the processing

machinery as opposed to when alpha is simply fluctuating with a random phase relation to input processing. In the latter case, alpha oscillations would form a pulsing filter that randomly amplifies or suppresses inputs, depending on when they arrive in the cortex.

Summary and Conclusion

This study used a set of active visual sampling paradigms that allow comparison of V1 excitability and stimulus processing both in the presence and absence of direct foveal input, thus isolating contextual eye movement-related signals. Our approach revealed a cyclical modulation of excitability in V1 that is tied to the fixation-saccade cycle; excitability and stimulus-evoked activity are enhanced immediately after fixation onset and this effect transitions to excitability and response suppression in the time leading up to the next saccade. Time-frequency decomposition suggests that the excitability modulation stems from a phase reset of ambient oscillatory activity in the delta-theta (2–6 Hz) range, accompanied by reset of harmonically unrelated activity in the alpha (8–13 Hz) range. These findings support two broad conclusions: (1) neuronal oscillations are instrumental to active visual processing and (2) accounting for eye movement dynamics and contextual influences is essential to a mechanistic understanding of visual information processing. As noted earlier (Schroeder et al., 2010; Lowet et al., 2018), both conclusions underscore the value of investigating vision within the active sensing framework.

STAR ★METHODS

CONTACT FOR REAGENT AND RESOURCE SHARING

Further information and data supporting the findings of this study are available upon reasonable request. All requests should be directed to and will be fulfilled by the Lead Contact, Charles Schroeder (charles.schroeder@nki.rfmh.org).

EXPERIMENTAL MODEL AND SUBJECT DETAILS

All procedures were approved in advance by the Animal Care and Use Committee of the Nathan Kline Institute. We report on electrophysiological data recorded during 70 penetrations (53 and 17 penetrations from Monkeys 1 and 2, respectively) of area V1 in two female monkeys (M. mulatta, 5.0–7.0 kg) that were obtained from an approved source.

METHOD DETAILS

Structural MRI and surgical preparation—Anatomical MRI scans were obtained using a 3 Tesla scanner with a transmission line coil optimized for the primate brain. Information from the MRI was used to guide the surgical placement of the recording chambers and to optimize the targeting of visual areas of the occipital lobe such that electrode penetrations could be made orthogonal to the laminar pattern (Schroeder et al., 1998; Chen et al., 2007).

The surgical procedure was performed using standard aseptic techniques under general anesthesia (Schroeder et al., 2001; Lakatos et al., 2013). The tissue overlying the calvarium was resected and appropriate portions of the cranium were removed. The neocortex and overlying dura were left intact. To allow electrode access to the brain and to promote an

orderly pattern of sampling across the surface of V1, custom recording chambers (Crist Instrument Co., Inc) incorporating electrode guide grids were placed over the craniotomies. These chambers and grids were angled so that the electrode track was perpendicular to the surface of V1, as determined by pre-implant MRI (Schroeder et al., 1998). The chambers, along with a titanium head post (Crist Instrument Co., Inc) used for painless head restraint, were secured to the skull with titanium orthopedic screws and embedded in bone cement. Plexiglass bars were embedded in bone cement for additional support during painless head restraint. A recovery time of six weeks was allowed before continuing any behavioral training and/or beginning data collection.

Behavioral training—Prior to surgery, each animal was adapted to a custom fitted primate chair and to the recording chamber. After the post-surgical recovery period, monkeys were acclimated to handling and sitting in their custom fitted chair. Animals were brought to the laboratory up to five times per week for training sessions. To decrease movement and accurately monitor eye position, once comfortable in the chair, monkeys were trained to allow their head to be painlessly restrained using the implanted headpost and/or embedded Plexiglas bars.

All tasks were performed in a sound attenuated chamber, lined with SONEX ProSPEC Composite™ sound absorbing foam. During recording, the only light source in the room was a CRT monitor. The eye-to-screen distance was 34.5 inches and the monitor encompassed 25.6° × 19° of visual space. Experiments were programmed and run using SR Research Experiment Builder (SR Research Ltd., Mississauga, Canada).

Free viewing task—Sets of twenty color images were randomly displayed twice for five seconds each. Between each image there was a three second black screen break. Color images were obtained from the internet (Google image searches). Each image was presented full screen (1024 × 768 pixels). There were no task instructions provided and no reward was delivered at any time. The monkey was free to make eye movements anywhere in the room–on or off the screen. To maintain a consistent level of engagement, each image was presented only twice during an experiment and new sets of images were rotated often.

Grey screen visual search task (GSS)—To isolate and analyze the effects of nonretinal input, this task was devised to get the monkeys to actively shift their gaze on a blank gray screen. To begin each trial, an array of four filled disks (5° diameter, 10.3° horizontal and 7° vertical separation) appeared on a uniform gray screen, initially at 3% contrast. The monkey’s task was to search for a hidden reward location by shifting gaze to each of the discs until the “target” was found. Target selection was signaled by the appearance of a small red dot, which was coupled with a juice reward. There were no cues identifying the target location; gaze had to move to each of the four discs until the target was found. Since the rate and location of eye movements was determined by each monkey, multiple eye movements could be made to any combination of disc location until target determination. As training progressed, the contrast between the disks and the background was decreased to zero and the monkey learned to continue making saccades to the remembered disc locations. During routine data collection sessions, the monkey was reminded of the disc locations briefly at the beginning of each trial, and the monkey

continued making saccades to the remembered locations on the blank gray screen. While the monkey performed the visual search task, large 19° Gabor patterns were flashed in the center of the screen. Responses to the Gabor flashes were used to assess the excitability of the system at different points during the saccade-fixation cycle (Figure 4). Flashes (35 ms duration) occurred independently of the monkeys' behavior, with up to six flashes during each trial. The inter-stimulus intervals were randomly distributed between 400 and 750 ms with a mean of 575 ms. For the analysis of eye-movement related activity without direct foveal stimulation (Figure 6), eye movements during which flashes occurred were excluded from the analysis.

Electrophysiological recordings—Experiments were conducted in an electrically shielded, sound-attenuated chamber. Recording electrodes had 23 contacts that were spaced either 100 or 200 μm apart (Plexon U-probe). Impedances ranged between 0.3–0.5 MΩ.

At the start of each experiment, flashes of diffuse light were used to elicit a visual evoked response profile in the cortex while the monkey sat in an otherwise completely dark recording chamber. These profiles were used to position the electrode to bracket the layers of V1 (Schroeder et al., 1998). The light flashes were generated by a Grass PS33 Plus Photic Stimulator (Grass-Telefactor Inc., West Warwick, RI) and projected onto a diffuser in front of the monkey at a viewing distance of 34 inches. Flashes occurred at 2 Hz and were each 10 ms in duration.

Data analysis—Neuroelectric signals were impedance matched with 10X gain pre-amplifiers situated on the electrode. After further amplification (500x), the signal was band-pass filtered into field potential (0.1–500 Hz) (Schroeder et al., 1991) and multiunit activity or "MUA" (0.2–5 kHz) ranges. Field potentials were sampled at 2 kHz per channel with 16-bit precision while MUA signals were sampled at 20 kHz per channel with 12-bit precision (LabView, National Instruments, Austin, TX). Data were stored for offline analysis. A continuous estimate of cell firing based on the MUA was obtained offline by further band-pass, zero phase shift digital filtering at 300–3,000 Hz and then rectification of the signal. Artifact-free epochs were averaged and CSD and MUA profiles were calculated using native and custom written MATLAB routines (MathWorks, Inc, Massachusetts). One-dimensional CSD profiles were calculated from the local field potential profiles using a three-point formula that calculates the second spatial derivative of voltage (Nicholson and Freeman, 1975; Schroeder et al., 1991). CSD analysis permits the examination of activity that occurred below the threshold for generating action potentials (Schroeder et al., 1998), provides a more direct index of the localized net transmembrane current flow, and is not affected by volume conduction like local field potentials (Mitzdorf, 1985; Schroeder et al., 1998; Kajikawa and Schroeder, 2011). To detail the cyclical nature of eye movement-related effects (Figure 4), for each layer and across all monkeys and GSS experiments, stimulus-related MUA was grouped according to the timing of fixation onset, averaged within each group, and then normalized to the MUA amplitude in grp4. Amplitude outliers outside of the y axis limits shown (.5 to 3.5) were included in the statistical analyses but are excluded from the figure. To examine CSD oscillations, a continuous wavelet transform was performed on data from each experiment, averaging over 600-ms bins surrounding each eye-movement

event. Instantaneous amplitude and phase were extracted using a Morlet wavelet. To characterize the phase distribution of oscillations, the wavelet-transformed single-trial data was averaged, and the mean length of the resulting vector was determined, which is a measure of inter-trial coherence (ITC). ITC values range from 0 to 1, with higher ITC values indicating that the observed oscillatory phase (at a given time-point across trials) is clustered more closely around the mean (i.e., non-uniform phase distribution). For eye movement data collected during free viewing and GSG tasks, amplitude and ITC values were compared during the 200 ms period before and 200 ms period after eye movement onset. Across experiments, these two periods were statistically evaluated using Wilcoxon rank sum tests. The analysis of saccade-related activity recorded in the dark was similar but for a 300 ms period before and after eye movement onset.

Laminar onset latency and depth of modulation—Signals were baseline corrected over the −20 ms to 20 ms period around each eye movement event of interest (fixation and saccade onsets). To calculate eye movement related laminar onset latency for each channel, CSD amplitudes were rectified and the mean and standard deviation of the baseline period were calculated. CSD onset was defined as the first 5ms period where the amplitude was at least five standard deviations greater than the mean of the baseline. To assess the eye movement related effects on local neuronal excitability, we calculated a “depth of modulation” value, defined as the difference between the baseline and the peak CSD amplitude from 0 to 300 ms after each eye movement event. Latency and amplitude values were calculated across channels for each run of free viewing and blank screen search. If more than one run of a task was performed during an electrode penetration, the onsets for each run were averaged so that there was only one set of values across channels per electrode penetration.

Gaze control and eye movement selection—Eye position was recorded with a 1.0-kHz sampling rate while monkeys performed the free viewing and gray screen visual search tasks using the EyeLink 1000 system (SR Research Ltd., Mississauga, Canada). Calibration of eye position used a 5-point system whereby the subject was trained to fixate on five circular targets displayed as a cross on the monitor. After calibration, eye-movement events (fixations, saccades, blinks) were determined and saved using SR Research software.

While there were no restrictions on where the monkeys could look during tasks, only the neural activity associated with eye movements that occurred on the central portion of the display monitor were analyzed (Figure 1A, yellow box). This region of interest was a 12.5° × 12.5° square, centered horizontally, and with the lower edge approximately 4° from the bottom of the screen. Based on the receptive field mapping (Figure 2), we selected experiments targeting portions of V1 that preferentially responded to the foveal/immediate foveal (1-3°) portion of visual space.

Receptive field mapping—Based on the pre-surgical anatomical MRI, we targeted chamber placement over the portion of V1 that contained a representation of the lower quadrant of the contralateral visual field. Utilizing a simple fixation paradigm, 1° portions of the lower contralateral visual field were systematically probed to map the receptive field properties of the neuronal population at each recording location. During this process, the

monkey was required to fixate on a low contrast 1° dot on the center of a black screen. At each trial, while fixation was maintained, up to two 1° white dots were flashed in two different positions on a 10° × 8° portion of the visual field being probed (Figure 2B). Each of the two white dots appeared for 35 ms with a 20-ms break between them. All flash evoked responses recorded from the granular layer were averaged and sorted based on stimulus location in the visual field. The resulting MUA color maps showed an area (relative to the center of the screen) where stimuli elicited a larger amplitude response (Figure 2C). Based on the anatomy and the receptive field determination, we could approximate the location of the horizontal and vertical meridians (Figure 2A, yellow and red lines, respectively). Anatomical examination post mortem confirmed the position of the chamber placement (Figure 2A, black circle).

QUANTIFICATION AND STATISTICAL ANALYSIS

The rate at which eye movements occur should center around a preferred frequency for each monkey. When comparing rate distributions between tasks and between monkeys, two-sample t tests were utilized. Since much of the electrophysiological data that we examine are not necessarily normally distributed, nonparametric statistical analyses were used whenever possible. When comparing the differences between onset latencies and depth of modulation amplitudes (Figure S1), we used the Kruskal-Wallis test followed by a multiple comparison analysis. Since the number of free viewing and blank screen search experiments differed, we used a two-sample t test to compare depth of modulation between tasks. The Kruskal-Wallis test followed by multiple comparisons analyses was also used when comparing the eye-movement related transient increase of excitability in Figure 4. To determine significant eye movement related ITC changes (Figures 5,6, and 7), ITC values within delta, theta, and alpha bands were compared before and after eye movement onset using Wilcoxon rank sum tests with a Bonferroni correction for multiple comparisons.

Supplementary Material

Refer to Web version on PubMed Central for supplementary material.

ACKNOWLEDGMENTS

This work was supported by National Institute of Mental Health grants R01-MH060358 and P50-MH109429. A.B. also received support from National Institute of Mental Health grant R01-MH109289, and S.H. was supported by Netherlands Organisation for Scientific Research Vidi grant 016.Vidi.185.137.

REFERENCES

Bastos AM, Loonis R, Kornblith S, Lundqvist M, and Miller EK (2018). Laminar recordings in frontal cortex suggest distinct layers for maintenance and control of working memory. Proc. Nat. Acad. Sci. U.S.A 115,1117–1122.

Bosman CA, Womelsdorf T, Desimone R, and Fries P (2009). A microsaccadic rhythm modulates gamma-band synchronization and behavior. J. Neurosci 29, 9471–9480. [PubMed: 19641110]

Bremmer F, Kubischik M, Hoffmann KP, and Krekelberg B (2009). Neural dynamics of saccadic suppression. J. Neurosci 29, 12374–12383. [PubMed: 19812313]

Burr DC, Morrone MC, and Ross J (1994). Selective suppression of the magnocellular visual pathway during saccadic eye movements. Nature 371, 511–513. [PubMed: 7935763]

Carracedo LM, Kjeldsen H, Cunnington L, Jenkins A, Schofield I, Cunningham MO, Davies CH, Traub RD, and Whittington MA (2013). A neocortical delta rhythm facilitates reciprocal interlaminar interactions via nested theta rhythms. J. Neurosci 33, 10750–10761. [PubMed: 23804097]

Casagrande VA (1994). A third parallel visual pathway to primate area V1. Trends Neurosci. 17, 305–310. [PubMed: 7524217]

Chen CM, Lakatos P, Shah AS, Mehta AD, Givre SJ, Javitt DC, and Schroeder CE (2007). Functional anatomy and interaction of fast and slow visual pathways in macaque monkeys. Cereb. Cortex 17, 1561–1569. [PubMed: 16950866]

Corbetta M, Akbudak E, Conturo TE, Snyder AZ, Ollinger JM, Drury HA, Linenweber MR, Petersen SE, Raichle ME, Van Essen DC, and Shulman GL (1998). A common network of functional areas for attention and eye movements. Neuron 21, 761–773. [PubMed: 9808463]

Deschênes M, Moore J, and Kleinfeld D (2012). Sniffing and whisking in rodents. Curr. Opin. Neurobiol 22, 243–250. [PubMed: 22177596]

Deubel H, Schneider WX, and Bridgeman B (1996). Postsaccadic target blanking prevents saccadic suppression of image displacement. Vision Res. 36, 985–996. [PubMed: 8736258]

Felleman DJ, and Van Essen DC (1991). Distributed hierarchical processing in the primate cerebral cortex. Cereb. Cortex 1, 1–47. [PubMed: 1822724]

Fiebelkorn IC, Saalmann YB, and Kastner S (2013). Rhythmic sampling within and between objects despite sustained attention at a cued location. Curr. Biol 23, 2553–2558. [PubMed: 24316204]

Fries W (1981). The projection from the lateral geniculate nucleus to the prestriate cortex of the macaque monkey. Proc. R. Soc. Lond. B Biol. Sci 213, 73–86. [PubMed: 6117869]

Gips B, van der Eerden JP, and Jensen O (2016). A biologically plausible mechanism for neuronal coding organized by the phase of alpha oscillations. Eur. J. Neurosci 44, 2147–2161. [PubMed: 27320148]

Givre SJ, Schroeder CE, and Arezzo JC (1994). Contribution of extrastriate area V4 to the surface-recorded flash VEP in the awake macaque. Vision Res. 34, 415–428. [PubMed: 8303826]

Haegens S, Nácher V, Luna R, Romo R, and Jensen O (2011). α-Oscillations in the monkey sensorimotor network influence discrimination performance by rhythmical inhibition of neuronal spiking. Proc. Natl. Acad. Sci. USA 108, 19377–19382. [PubMed: 22084106]

Haegens S, Barczak A, Musacchia G, Lipton ML, Mehta AD, Lakatos P, and Schroeder CE (2015). Laminar Profile and Physiology of the α Rhythm in Primary Visual, Auditory, and Somatosensory Regions of Neocortex. J. Neurosci 35, 14341–14352. [PubMed: 26490871]

Hatsopoulos NG, and Suminski AJ (2011). Sensing with the motor cortex. Neuron 72, 477–487. [PubMed: 22078507]

Hendry SH, and Reid RC (2000). The koniocellular pathway in primate vision. Annu. Rev. Neurosci 23, 127–153. [PubMed: 10845061]

Hendry SHC, and Yoshioka T (1994). A neurochemically distinct third channel in the macaque dorsal lateral geniculate nucleus. Science 264, 575–577. [PubMed: 8160015]

Hoffman JE, and Subramaniam B (1995). The role of visual attention in saccadic eye movements. Percept. Psychophys 57, 787–795. [PubMed: 7651803]

Ibbotson M, and Krekelberg B (2011). Visual perception and saccadic eye movements. Curr. Opin. Neurobiol 21, 553–558. [PubMed: 21646014]

Ito J, Maldonado P, Singer W, and Grün S (2011). Saccade-related modulations of neuronal excitability support synchrony of visually elicited spikes. Cereb. Cortex 21, 2482–2497. [PubMed: 21459839]

Jeannerod M, Kennedy H, and Magnin M (1979). Corollary discharge: its possible implications in visual and oculomotor interactions. Neuropsychologia 17, 241–258. [PubMed: 223083]

Jensen O, and Mazaheri A (2010). Shaping functional architecture by oscillatory alpha activity: gating by inhibition. Front. Hum. Neurosci 4, 186. [PubMed: 21119777]

Jones EG (2001). The thalamic matrix and thalamocortical synchrony. Trends Neurosci. 24, 595–601. [PubMed: 11576674]

Kajikawa Y, and Schroeder CE (2011). How local is the local field potential? Neuron 72, 847–858. [PubMed: 22153379]

Kayser C, Montemurro MA, Logothetis NK, and Panzeri S (2009). Spike-phase coding boosts and stabilizes information carried by spatial and temporal spike patterns. Neuron 61, 597–608. [PubMed: 19249279]

Kleinfeld D, Ahissar E, and Diamond ME (2006).Active sensation: insights from the rodent vibrissa sensorimotor system. Curr. Opin. Neurobiol 16, 435–444. [PubMed: 16837190]

Lakatos P, Karmos G, Mehta AD, Ulbert I, and Schroeder CE (2008). Entrainment of neuronal oscillations as a mechanism of attentional selection. Science 320, 110–113. [PubMed: 18388295]

Lakatos P, Musacchia G, O'Connel MN, Falchier AY, Javitt DC, and Schroeder CE (2013). The spectrotemporal filter mechanism of auditory selective attention. Neuron 77, 750–761. [PubMed: 23439126]

Landau AN, and Fries P (2012). Attention samples stimuli rhythmically. Curr. Biol 22, 1000–1004. [PubMed: 22633805]

Lee D, and Malpeli JG (1998). Effects of saccades on the activity of neurons in the cat lateral geniculate nucleus. J. Neurophysiol 79, 922–936. [PubMed: 9463453]

Lee JH, Whittington MA, and Kopell NJ (2013). Top-down beta rhythms support selective attention via interlaminar interaction: a model. PLoS Comput. Biol 9, e1003164. [PubMed: 23950699]

Lowet E, Roberts MJ, Peter A, Gips B, and DeWeerd P (2017).A quantitative theory of gamma synchronization in macaque V1. eLife 6, e26642. [PubMed: 28857743]

Lowet E, Gomes B, Srinivasan K, Zhou H, Schafer RJ, and Desimone R (2018). Enhanced Neural Processing by Covert Attention only during Microsaccades Directed toward the Attended Stimulus. Neuron 99,207–214.e3. [PubMed: 29937279]

Maldonado P, Babul C, Singer W, Rodriguez E, Berger D, and Grün S (2008). Synchronization of neuronal responses in primary visual cortex of monkeys viewing natural images. J. Neurophysiol 100, 1523–1532. [PubMed: 18562559]

Mathewson KE, Lleras A, Beck DM, Fabiani M, Ro T, and Gratton G (2011). Pulsed out of awareness: EEG alpha oscillations represent a pulsed-inhibition of ongoing cortical processing. Front. Psychol 2, 99. [PubMed: 21779257]

Maunsell JHR, and Gibson JR (1992). Visual response latencies in striate cortex of the macaque monkey. J. Neurophysiol 68, 1332–1344. [PubMed: 1432087]

McConkie GW, and Loschky LC (2002). Perception onset time during fixations in free viewing. Behav. Res. Methods Instrum. Comput 34, 481–490. [PubMed: 12564552]

McFarland JM, Bondy AG, Saunders RC, Cumming BG, and Butts DA (2015). Saccadic modulation of stimulus processing in primary visual cortex. Nat. Commun 6, 8110. [PubMed: 26370359]

Mehta AD, Ulbert I, and Schroeder CE (2000a). Intermodal selective attention in monkeys. II: physiological mechanisms of modulation. Cereb. Cortex 10, 359–370. [PubMed: 10769248]

Mehta AD, Ulbert I, and Schroeder CE (2000b). Intermodal selective attention in monkeys. I: distribution and timing of effects across visual areas. Cereb. Cortex 10, 343–358. [PubMed: 10769247]

Melloni L, Schwiedrzik CM, Rodriguez E, and Singer W (2009). (Micro) Saccades, corollary activity and cortical oscillations. Trends Cogn. Sci 13, 239–245. [PubMed: 19428286]

Mitzdorf U (1985). Current source-density method and application in cat cerebral cortex: investigation of evoked potentials and EEG phenomena. Physiol. Rev 65, 37–100. [PubMed: 3880898]

Morillon B, Schroeder CE, and Wyart V (2014). Motor contributions to the temporal precision of auditory attention. Nat. Commun 5, 5255. [PubMed: 25314898]

Morris AP, Kubischik M, Hoffmann KP, Krekelberg B, and Bremmer F (2012). Dynamics of eye-position signals in the dorsal visual system. Curr. Biol 22, 173–179. [PubMed: 22225775]

Morrocco R, and McKlurkin J (1982). Spatial summation and conduction latency classsification of cells in the lateral geniculate nucleus of maccaques. J. Neurosci 9, 1275–1291.

Nicholson C, and Freeman JA (1975). Theory of current source-density analysis and determination of conductivity tensor for anuran cerebellum. J. Neurophysiol 38, 356–368. [PubMed: 805215]

Nobre A, Correa A, and Coull J (2007). The hazards of time. Curr. Opin. Neurobiol 17, 465–470. [PubMed: 17709239]

Noudoost B, Chang MH, Steinmetz NA, and Moore T (2010). Top-down control of visual attention. Curr. Opin. Neurobiol 20, 183–190. [PubMed: 20303256]

Purpura KP, Kalik SF, and Schiff ND (2003). Analysis of perisaccadic field potentials in the occipitotemporal pathway during active vision. J. Neurophysiol 90, 3455–3478. [PubMed: 12878708]

Rajkai C, Lakatos P, Chen CM, Pincze Z, Karmos G, and Schroeder CE (2008). Transient cortical excitation at the onset of visual fixation. Cereb. Cortex 18, 200–209. [PubMed: 17494059]

Reppas JB, Usrey WM, and Reid RC (2002). Saccadic eye movements modulate visual responses in the lateral geniculate nucleus. Neuron 35, 961–974. [PubMed: 12372289]

Saalmann YB, Pinsk MA, Wang L, Li X, and Kastner S (2012). The pulvinar regulates information transmission between cortical areas based on attention demands. Science 337, 753–756. [PubMed: 22879517]

Schiller PH, and Colby CL (1983). The responses of single cells in the lateral geniculate nucleus of the rhesus monkey to color and luminance contrast. Vision Res. 21, 1631–1641.

Schroeder CE, and Lakatos P (2009). Low-frequency neuronal oscillations as instruments of sensory selection. Trends Neurosci. 32, 9–18. [PubMed: 19012975]

Schroeder CE, Tenke CE, Arezzo JC, and Vaughan HG Jr. (1989). Timing and distribution of flash-evoked activity in the lateral geniculate nucleus of the alert monkey. Brain Res. 477, 183–195. [PubMed: 2702483]

Schroeder CE, Tenke CE, Givre SJ, Arezzo JC, and Vaughan HG Jr. (1991). Striate cortical contribution to the surface-recorded pattern-reversal VEP in the alert monkey. Vision Res. 31, 1143–1157. [PubMed: 1891808]

Schroeder CE, Mehta AD, and Givre SJ (1998). A spatiotemporal profile of visual system activation revealed by current source density analysis in the awake macaque. Cereb. Cortex 8, 575–592. [PubMed: 9823479]

Schroeder CE, Lindsley RW, Specht C, Marcovici A, Smiley JF, and Javitt DC (2001). Somatosensory input to auditory association cortex in the macaque monkey. J. Neurophysiol 85, 1322–1327. [PubMed: 11248001]

Schroeder CE, Wilson DA, Radman T, Scharfman H, and Lakatos P (2010). Dynamics of Active Sensing and perceptual selection. Curr. Opin. Neurobiol 20, 172–176. [PubMed: 20307966]

Sheliga BM, Riggio L, and Rizzolatti G (1994). Orienting of attention and eye movements. Exp. Brain Res 98, 507–522. [PubMed: 8056071]

Sherman SM, and Guillery RW (2002). The role of the thalamus in the flow of information to the cortex. Philos. Trans. R. Soc. Lond. B Biol. Sci 357,1695–1708. [PubMed: 12626004]

Sommer MA, and Wurtz RH (2008). Visual perception and corollary discharge. Perception 37, 408–418. [PubMed: 18491718]

Vijayan S, and Kopell NJ (2012). Thalamic model of awake alpha oscillations and implications for stimulus processing. Proc. Natl. Acad. Sci. USA 109,18553–18558. [PubMed: 23054840]

Wurtz RH, and Sommer MA (2004). Identifying corollary discharges for movement in the primate brain. Prog. Brain Res 144, 47–60. [PubMed: 14650839]

Yarbus AL (1967). Eye Movements and Vision (Plenum Press).

Yukie M, and Iwai E (1981). Direct projection from the dorsal lateral geniculate nucleus to the prestriate cortex in macaque monkeys. J. Comp. Neurol 201, 81–97. [PubMed: 7276252]

Zanos TP, Mineault PJ, Nasiotis KT, Guitton D, and Pack CC (2015). A sensorimotor role for traveling waves in primate visual cortex. Neuron 85, 615–627. [PubMed: 25600124]

Zanos TP, Mineault PJ, Guitton D, and Pack CC (2016). Mechanisms of Saccadic Suppression in Primate Cortical Area V4. J. Neurosci 36, 9227–9239. [PubMed: 27581462]

Highlights

- Active visual sensing differs from visual processes studied in traditional tasks
- Rhythmic patterns of fixations and saccades contextually modulate visual processing
- Eye movement-related modulation increases excitability just after fixation onset
- Enhancement and suppression cycle is tied to the phase reset of neuronal oscillations

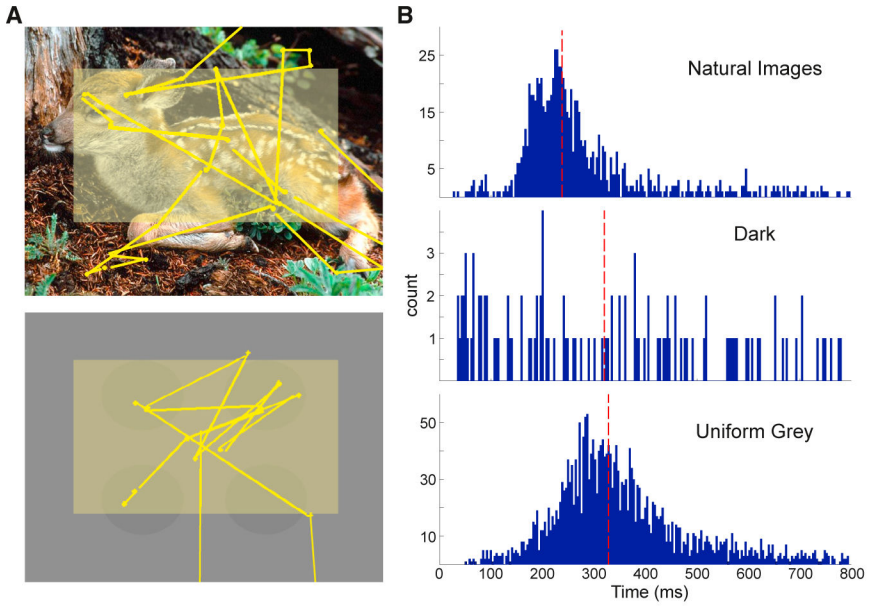

Figure 1. Eye Movement Dynamics across Tasks

(A) Sample screen images displayed during FV (top) and GSS (bottom) with representative scan patterns overlaid. Yellow dots and lines represent the locations of fixations and saccades, respectively. Faded yellow rectangle depicts the region of the screen where eye movements were analyzed.

(B) Representative ISacI distributions during sample sessions of FV (top, n = 839), dark (center, n = 112), and GSS tasks (bottom, n = 2,441). Dashed vertical red lines depict the median ISacI of each representative distribution.

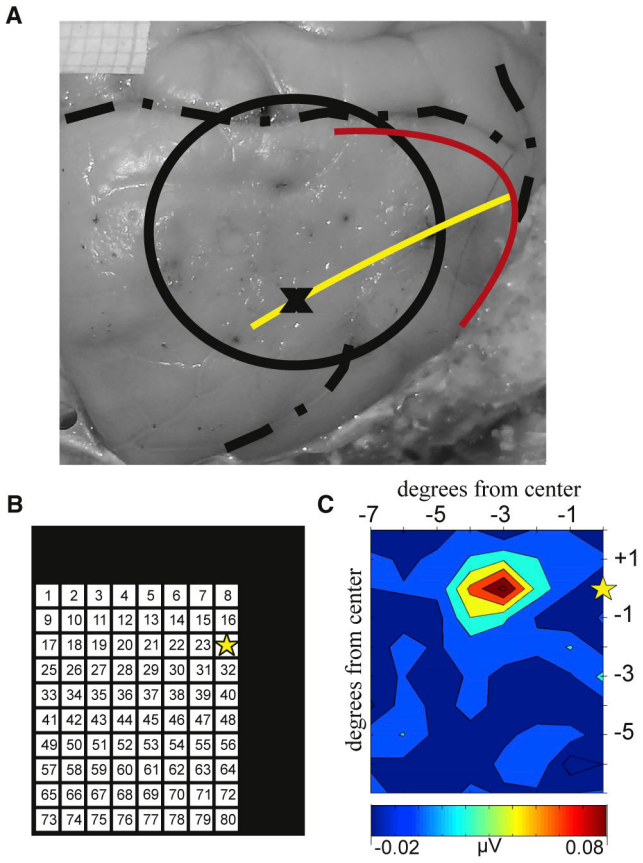

Figure 2. Receptive Field Mapping

(A) Photograph of the surface of the right occipital cortex. The circle indicates the chamber location. The red and yellow lines indicate the approximate location of the vertical and horizontal meridians, respectively. The black X is the approximate recording location for the receptive field example shown.

(B) Location map for the receptive field paradigm. The black box depicts a portion of the screen display. The 8° × 10° matrix indicates locations where the 1° solid white circle flashes occurred while mapping the population receptive field at the electrode location, "X." The yellow star indicates the center of the screen, where fixation was held.

(C) Representative MUA map summarizing the receptive field for the neuronal population in the granular layer of the example recording site.

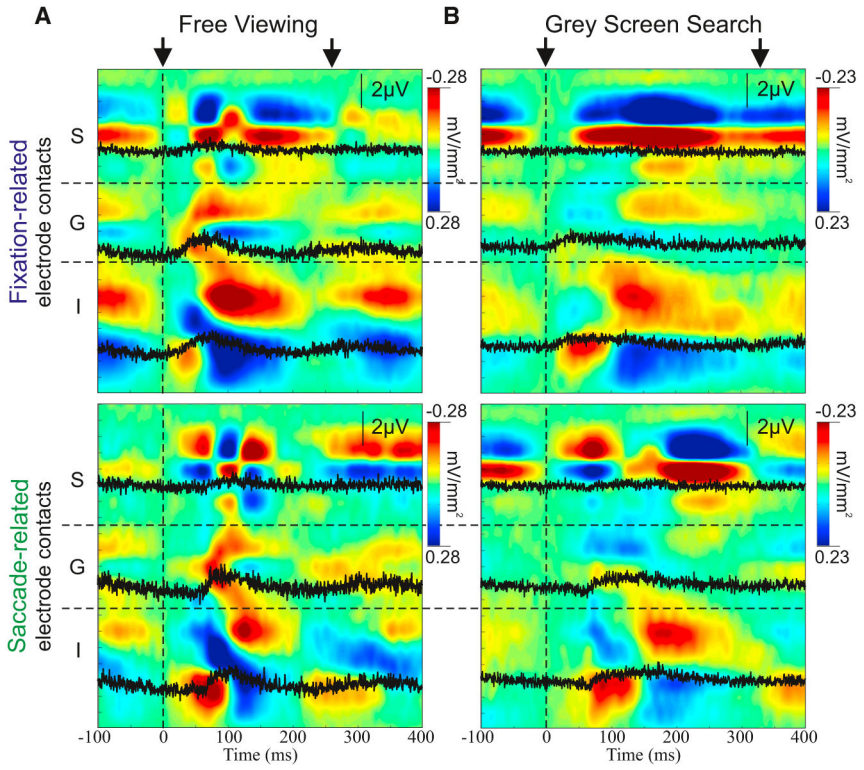

Figure 3. Representative Eye Movement-Related Laminar CSD Profiles

(A) CSD profiles (extracellular current sinks and sources in red and blue, respectively) aligned to fixation (top) and saccade onsets (bottom) for eye movements during the FV task. Three representative MUA channels within supragranular (S), granular (G), and infragranular (I) layers are overlaid in black. Black arrows at the top indicate the timing of the initial and approximate successive eye movements based on the median ISacI.

(B) Similar to (A) for eye movements occurring during GSS.

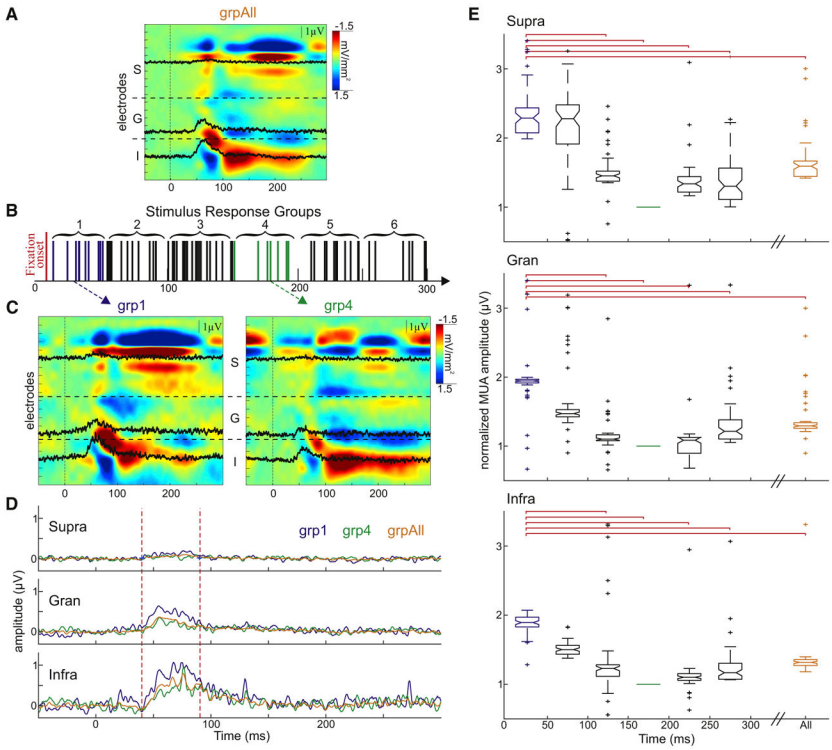

Figure 4. Eye Movement-Related Transient Increase in Excitability

(A) Example laminar CSD profiles for pattern-evoked responses in grpAll aligned to stimulus onset with representative MUA channels overlaid in black.

(B) Schematic depiction of the grouping of pattern-evoked responses according to the period of time between fixation and stimulus onset.

(C) Example CSD response profiles for grp1 (left) and grp4 (right). Vertical lines at 0 ms denote stimulus onset.

(D) Representative comparison between the average supragranular (top), granular (center), and infragranular (bottom) MUA responses to stimuli from grp1 (blue), grp4 (green), and grpAll (orange). Vertical dashed lines indicate time period used for statistical comparisons of the grouped data presented in (E).

(E) Normalized, averaged pattern-evoked MUA amplitudes for all of the experiments across the supragranular (top), granular (center), and infragranular (bottom) layers for each of the seven stimulus response groups. Red brackets indicate significant difference between groups. For all layers: grp1 versus 2 p = NS, grp1 versus grp3 $p < 0.001$, grp1 versus grp4 $p < 0.001$, grp1 versus grp5 $p < 0.001$, and grp1 versus grp6 $p < 0.001$.

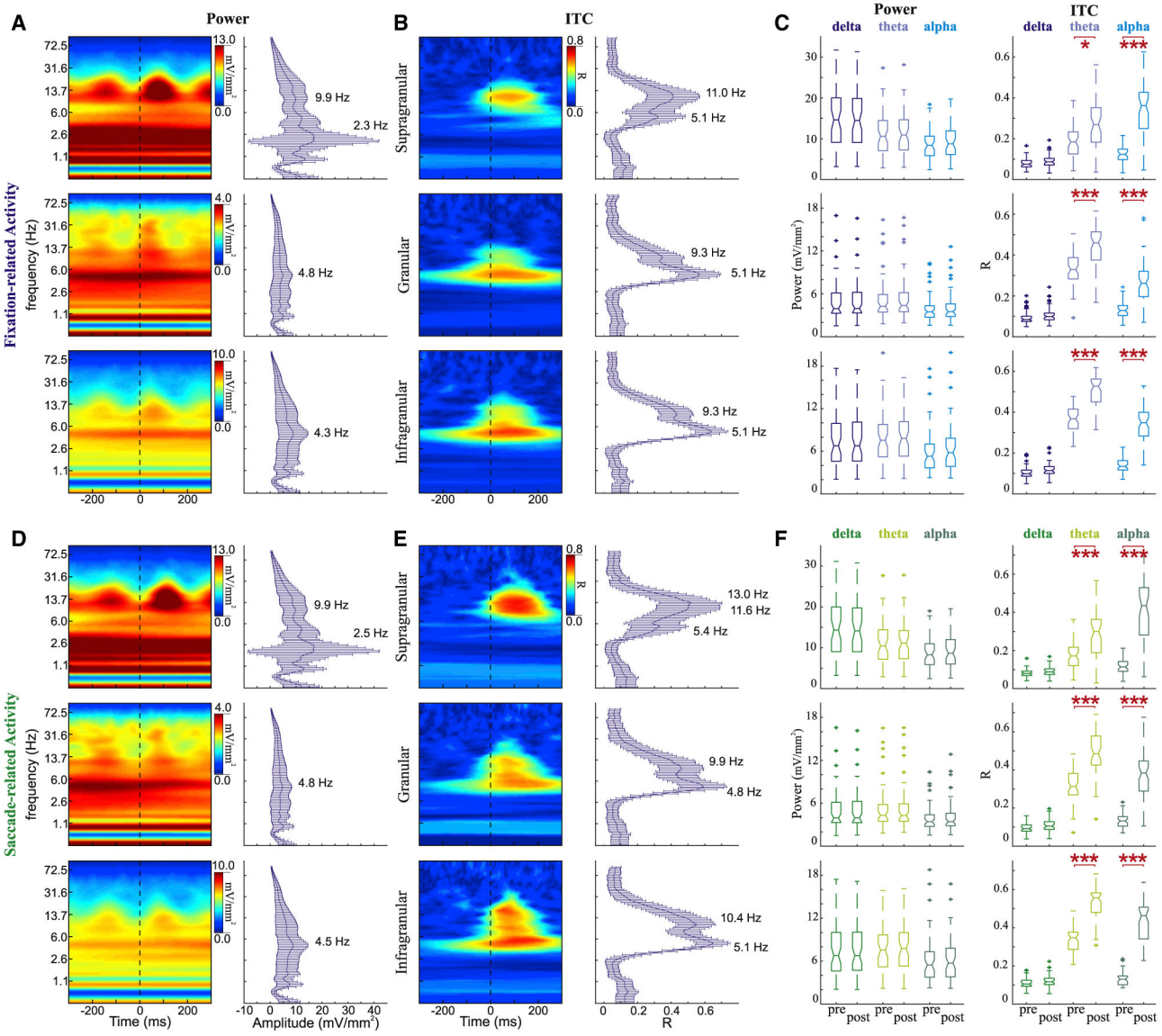

Figure 5. Spectrotemporal Profiles of Eye Movement Events during FV

(A) Example power spectra (left) for fixation-related activity aligned to fixation onset for supragranular (top), granular (center), and infragranular (bottom) layers. Frequency plots with error bars (right) show medians and SDs of power across all experiments (supra n = 52, gran and infra n = 58) at each frequency measured at the timing of the broadband power peak.

(B) Example ITC profiles (left) for fixation-related activity aligned to fixation onset for supragranular (top), granular (center), and infragranular (bottom) layers. Frequency plots with error bars (right) show median ITC across all experiments at each frequency measured at the timing of the broadband power peak.

(C) Boxplots statistically comparing power (left) and ITC (right) during the 200 ms period before and the 200 ms period after fixation onset. Horizontal red lines signify a significant difference pre-versus post-eye movement onset (Wilcoxon rank-sum tests with Bonferroni correction, *$p < 0.05$, **$p < 0.01$, and ***$p < 0.001$).

(D–F) Saccade-related activity described with the same conventions as in (A) for power profiles (D), as in (B) for ITC profiles (E), and as in (C) for statistical comparisons across experiments (F).

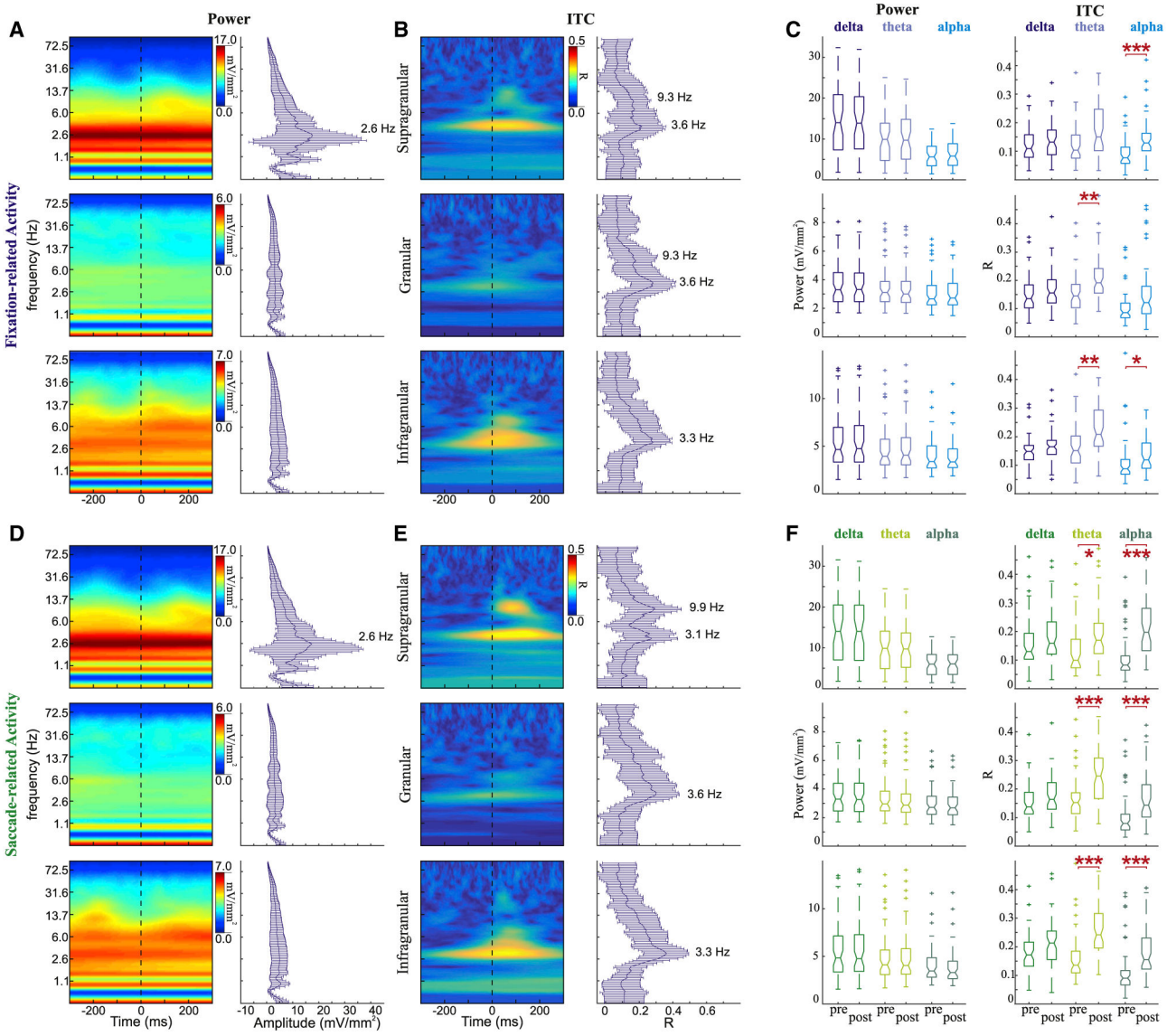

Figure 6. Spectrotemporal Profiles of Eye Movement Events during GSS

(A) Example power spectra (left) for fixation-related activity aligned to fixation onset for supragranular (top), granular (middle), and infragranular (bottom) layers. Frequency plots with error bars (right) show median and SD of power across all experiments (supra n = 55; gran and infra n = 60) at each frequency measured at the timing of the broadband power peak.

(B) Example ITC profiles (left) for fixation-related activity aligned to fixation onset for supragranular (top), granular (middle), and infragranular (bottom) layers. Frequency plots with error bars (right) show median ITC across all experiments at each frequency measured at the timing of the broadband power peak.

(C) Boxplots statistically comparing power (left) and ITC (right) during the 200 ms period before and 200 ms period after fixation onset. Horizontal red lines signify a significant difference pre- vs post-eye movement onset (Wilcoxon rank-sum tests with Bonferroni correction, *$p < 0.05$, **$p < 0.01$, ***$p < 0.001$).

(D–F) Saccade-related activity described with the same conventions as in (A) for power profiles (D), as in (B) for ITC profiles (E), and as in (C) for statistical comparisons across experiments (F).

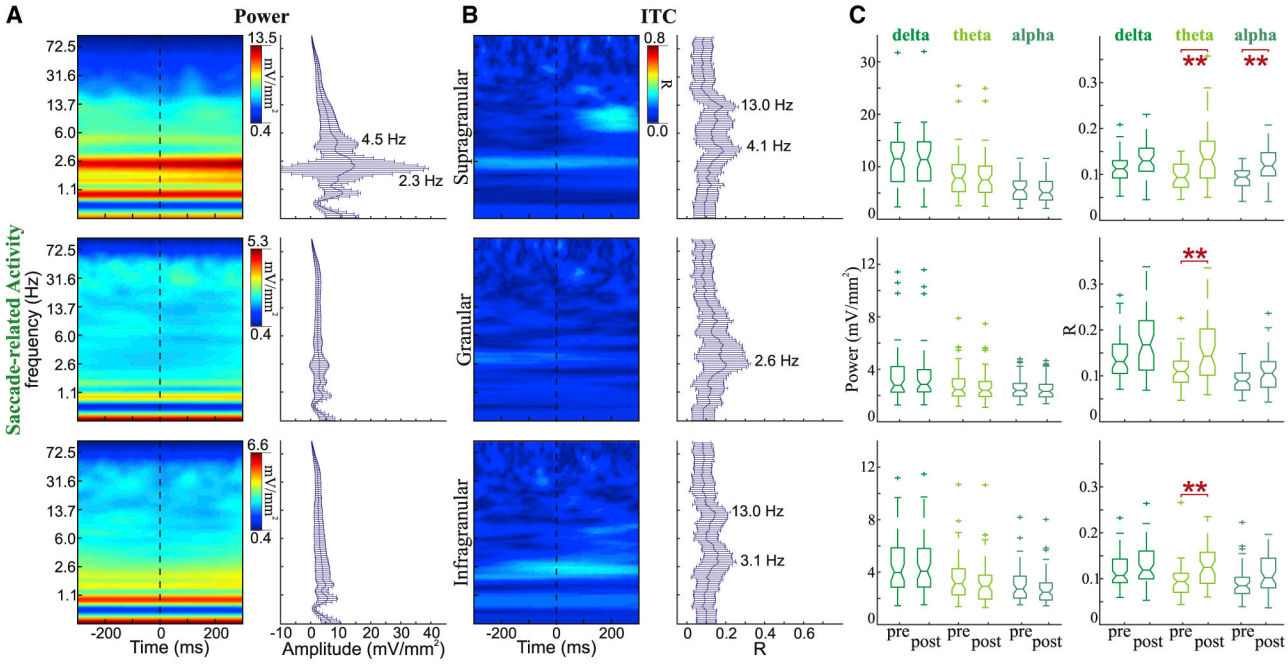

Figure 7. Spectrotemporal Profiles of Saccades Made in the Dark

(A) Example power spectra (left) for saccade-related activity aligned to saccade onset for supragranular (top), granular (middle), and infragranular (bottom) layers. Frequency plots with error bars (right) show median and SD of power across all experiments (supra n = 49; gran and infra n = 56) at each frequency measured at the timing of the broadband power peak.

(B) Saccade-related ITC activity described with the same conventions as in (A) for ITC profiles.

(C) Boxplots statistically comparing power (left) and ITC (right) during the 300 ms period before and 300 ms period after fixation onset. Horizontal red lines signify a significant difference pre- versus post-saccade onset (Wilcoxon rank-sum tests with Bonferroni correction, *$p < 0.05$, **$p < 0.01$, and ***$p < 0.001$).

KEY RESOURCES TABLE

REAGENT or RESOURCE	SOURCE	IDENTIFIER
Experimental Models: Organisms/Strains		
Macaque monkeys	Alpha Genesis Inc.	http://www.alphagenesisinc.com/
Software and Algorithms		
Experiment Builder	SR Research Ltd.	https://www.sr-research.com/
Data Viewer	SR Research Ltd.	https://www.sr-research.com/
MATLAB	MathWorks	https://www.mathworks.com/
Other		
Recording chambers, grids, and head post	Crist Instrument Co., Inc	http://www.cristinstrument.com/
EyeLink 1000 system	SR Research Ltd.	https://www.sr-research.com/
Recording electrodes	Plexon	https://plexon.com/